Scalable Cylindrical Metallodielectric Metamaterials

By *Nicholas Gibbons,* Jeremy J. Baumberg,* Chris L. Bower, Mathias Kolle,* and *Ullrich Steiner*

Much interest has been shown recently in metallodielectric multilayer structures due to their potential for near-field imaging and lithography applications in the visible region of the spectrum. It was originally proposed that a single silver layer could be used as a flat lens for a single polarization[1] focusing incident light to an image by negative refraction. Additionally, such a lens was predicted to support the evanescent modes of an image, thus bypassing the resolution limit experienced by conventional lenses. The normally evanescent sub-wavelength details of an image are able to couple with the surface plasmons that reside upon the metal layer and are sustained resonantly through the slab. This has huge implications in near-field microscopy, where it could be used to uncover details that are not possible to resolve with conventional lenses. However, in practice, this simple system has serious limitations due to the large absorption of metals in the visible region, where the skin depth of gold and silver is around 10 nm. Consequently, an improved performance was suggested based on a periodic stack of metal and dielectric layers.[2] Since the evanescent components of an image undergo periodic amplification and decay at each interface within the multilayer, the field intensity is prevented from becoming too high at any point within the medium, and hence the resolution is improved. As the thickness, t, of these layers decreases ($t \ll \lambda$), the effective medium approximation becomes valid and the metamaterial can then be described by the macroscopic optical parameters, ε and μ. However, effective fabrication of appropriate structures is currently the focus of active research.

Traditionally, such multilayers required vacuum deposition and utilized only small areas, limiting their potential application. Although two-source sputtering has been used to effectively fabricate bimetallic X-ray mirrors with up to 100 layers,[3] this process requires significant time and cost. Two-source sputtering has also been used to fabricate Ag/MgF_2 superlenses consisting of 16 curved layers;[4] however, these structures are inherently brittle, and their fabrication is hard to control, slow, and expensive. Metal–semiconductor multilayers have also been constructed, where a lattice-mismatched semiconductor bilayer leads to induced roll-up.[5,6] Unfortunately, this approach has severe limitations in the choice of layer thicknesses and of materials (which have to be grown by molecular beam epitaxy in specific alloy combinations). With layers thicker than 20 nm, strain relaxation occurs, leading to misfit dislocations that tear the top semiconductor layer apart. It would thus be very desirable to fabricate similar structures from flexible materials such as polymers, extending their potential applicability greatly and allowing scale-up of metamaterials fabrication for the first time.

Here, we demonstrate a new and significantly more adaptable approach to the fabrication of multilayer metamaterials by growing a single metal–polymer bilayer and rolling it up around a central rod. Since the entire structure comes from a single bilayer, uniformity can be better controlled than successive depositions. This approach allows a wide range of different materials with arbitrary layer thicknesses. Structures demonstrated here are Bragg arranged by design, allowing us to exploit the high sensitivity of the reflection resonances to thickness variations in the layers, and therefore to accurately quantify the conformity of our multilayers. Such Bragg-arranged metallodielectrics have additional properties, such as enhanced transmission and reflection at particular resonant frequencies,[7–9] which can be exploited as a route towards transmissive, nonlinear composite materials.[10] Furthermore, when arranged appropriately, these structures can allow the propagation of both the low and high wavevector components of an image over the entire visible spectrum, which could ultimately lead to broad-band imaging properties. Our approach has the potential to offer a fully mass-scalable route to 2D and 3D metamaterials from flexible components.

These periodic stacks have been shown to exhibit an anisotropic permittivity,[11] which supports propagation of the elusive, evanescent modes of an image along a preferred direction, as in a waveguide. By careful choice of the layers' thickness ratio, one component of its effective permittivity tensor becomes opposite in sign to the others over a range of frequencies. Normally, decaying components with high wavevectors propagate within the multilayer through plasmonic coupling at the surfaces of the metal layers, and they are guided by negative refraction. This allows the subwavelength details of an image to be focused through such a stack, revealing previously obscured details down to $\lambda/12$.[4,12–14] Waves propagating through these media experience a group velocity that is opposite in direction to their phase velocity, leading to a reversal of Snell's law[15] and hence, negative refraction. It should be noted that even

[*] N. Gibbons, Prof. J. J. Baumberg
Nanophotonics Centre
University of Cambridge
Cambridge CB3 OHE (UK)
E-mail: ng322@cam.ac.uk; jjb12@cam.ac.uk
Dr. C. L. Bower
Kodak European Research
332 Science Park
Cambridge CB4 0WN (UK)
M. Kolle, Prof. U. Steiner
Biological and Soft Systems Group
University of Cambridge
Cambridge CB3 0HE (UK)

DOI: 10.1002/adma.200900461

though these structures can exhibit negative refraction, technically they are not negative-index materials, due to the lack of a negative μ. The large intensities arising within the medium due to negative refraction can also lead to strong nonlinear effects, such as second-harmonic generation and stimulated Raman scattering, which have been recently discussed in the literature.[16,17] It has also been proposed that backwards optical parametric amplification could be utilized to counteract absorption losses within these media.

Fabrication involves deposition of a single polymer–metal bilayer that is then floated off and captured on a meniscus. Subsequent float-rolling defines the final cylindrical structure. A flat silicon substrate is spin coated with a 0.8 μm layer of polystyrene sulfonic acid (PSS), which is used as a sacrificial layer in the film lift-off. The sample is then spin coated with a 160 nm layer of polystyrene (PS) using atomic force miscroscopy (AFM) to calibrate the spin-coater parameters. A 10 nm gold layer is finally vacuum evaporated onto the PS surface, completing the metallodielectric bilayer (Fig. 1a). The edges of the films are defined by making sharp cuts across the face of the sample to give separate, rectangular films, each having dimensions of 66 mm × 22 mm. These films are floated from the substrate by dissolving the sacrificial layer in water. Once the films are free from the substrate, they are supported by the surface tension of the water and can be rolled up around cylindrical quartz rods of 2 mm diameter. The films are rolled up in a helical fashion, allowing optical access to different numbers of layers within the multilayer (Fig. 1b). The completed roll structure (Fig. 1c and d) appears strongly iridescent as expected, with different colors apparent at different points along the helix, and only small number of defects.

AFM scans of the PS and Au layers were taken during the fabrication process in order to record their surface roughness (Fig. 2a). The PS layer has an RMS height variation of ≤1 nm and the Au surface has an RMS height variation of ≤2 nm along a 10 μm line across the face of the sample. To check the uniformity of the films, one of them was floated onto a glass microscope slide and reflection spectra were taken across the face of the film at 5 mm separations (Fig. 2b). There is good consistency with transfer matrix simulations, exhibiting the expected dip in reflection at 500 nm corresponding to the increased absorption at

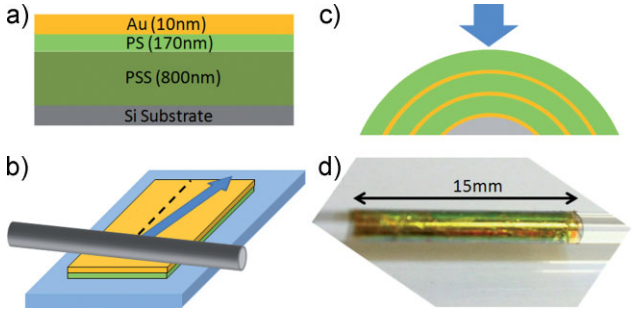

Figure 1. a) Sample prior to rolling. b) After lifting from the substrate, the film is adhered to the glass rod and rolled up in the direction shown. c) One cross-sectioned hemisphere of the final structure. Light is incident normal to the plane of the layers. d) Photograph of a finished polymer roll. Diameter of the rod is 2 mm.

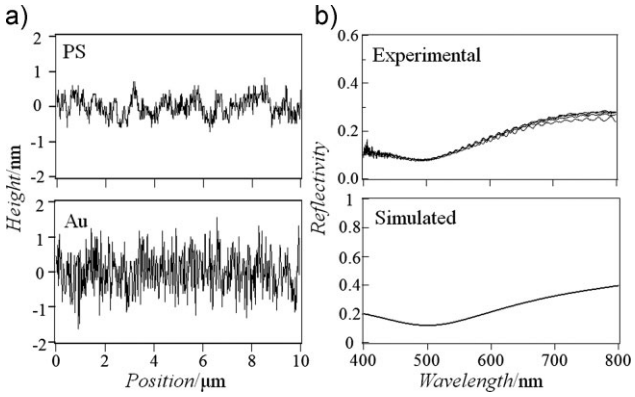

Figure 2. a) AFM images show height variation across 10 μm cross-sections of the PS and Au surfaces. b) Reflection spectra taken at five points across the face of a single bilayer and transfer matrix simulations of a corresponding bilayer.

the plasma frequency of gold. The uniformity of the gold layer is quantified by the variation of the peak reflectivity at each point, and its thickness is found to vary by less than 1 nm across the sample width.

The polymer rolls were dried and then characterized optically using a microscope and spectrometer system. A 20× objective was used, producing a spot size of 20 μm that allows us to ignore the effect of surface curvature. Reflection spectra are taken across the top surface of the sample. These spectra are compared to identify the number of layers that are present at each point within the helical layering system shown in Figure 3a. In order to minimize losses arising from the cylindrical geometry, measurements were only taken along the central axis of the roll and normalized against the center of the bare glass rod.

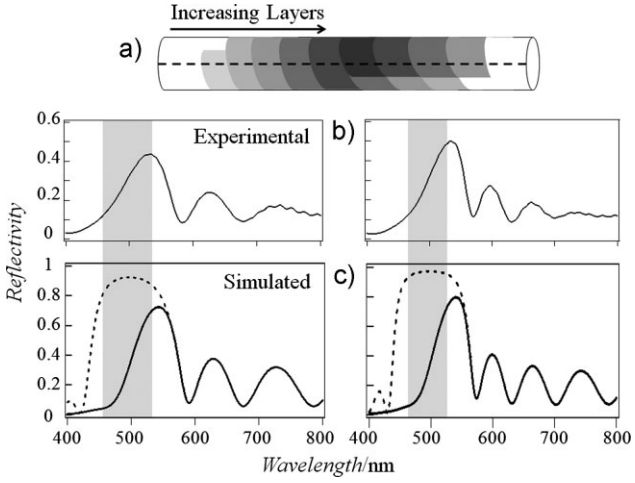

Figure 3. a) Helical roll-up was employed to enable access to different numbers of layers. Spectra were only taken along the dashed line. b) Experimental reflection spectra for six and eight layer points upon the polymer roll. Bragg stopbands are shown by the shaded areas. c) Simulated reflection spectra for six and eight flat bilayers of 160 nm PS and 10 nm Au. Rectangular stopbands arising from a purely dielectric multilayer stack are shown for an equivalent number of layers (dashed line).

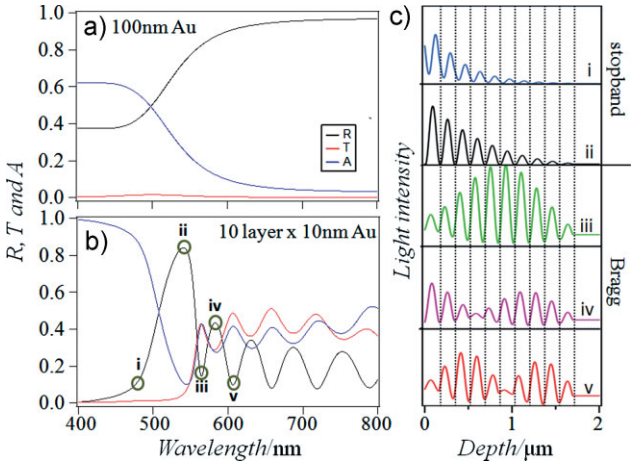

Figure 4. Transfer matrix simulations showing reflection (R), transmission (T) and absorption (A) of a) a 100 nm block of Au and b) a ten layer PS/Au stack. c) Electric field distribution inside the structure can be seen for different Bragg resonances within the visible. Dashed lines indicate the position of the Au layers. i) Maximum absorption. ii) First photon bandgap mode (PBM) mode. iii) First Bragg mode. iv) Second PBG mode. v) Second Bragg mode.

The agreement between the experimental and simulated data (Fig. 3b and c) is very encouraging: the frequency of the Bragg resonances fit well with calculations, and they can be seen clearly to sharpen as the number of layers increases. The absolute reflectivity of our multilayer is not as high as predicted by simulations, which could be influenced by even a small degree of surface roughness, leading to additional scattering losses. The shaded bands mark the position of the Bragg reflection stopbands with no absorption in the multilayer, and rectangular Bragg stopbands are also shown for equivalent purely dielectric structures (Fig. 3c). When absorption in the Au is included, the spectral shape of the stopband changes from rectangular to triangular. The origin of this change in spectral shape can be understood from mapping the optical field at the resonances. The separation of 100 nm Au into ten Bragg-spaced layers traps the light in different configurations (Fig. 4). The triangular stopband arises because on the long-wavelength side (when the experimental absolute reflectivity exceeds 50%), the electric field fits within the structure, such that it avoids the Au layer completely (Fig. 4c ii). Absorption can be minimized in this way, and so high reflection is seen at all frequencies where the field envelope can fit $n+1/2$ times within the stack (Fig. 4c ii and iv). In contrast, on the short-wavelength side, the electric field is concentrated in the gold, leading to high absorption (Fig. 4c i).

Bragg transmission resonances are also present (Fig. 4c iii and iv), corresponding to the points of minimum reflection, and they occur whenever the field envelope can fit n times within the stack, maximizing transmission of the light. Remarkably, 50% transmission is observed at the second Bragg resonance, through a total of 100 nm of gold, whilst the equivalent transmission through a 100 nm single block of gold is 160 times smaller. We believe the deviance from our predicted reflectivity of $\geq$60% (Fig. 3b and c) is due to the extreme sensitivity of the optical tunneling to imperfections in the gold/polymer interfaces, thicknesses, and scattering.

We have shown in this communication an effective technique for the fabrication of metallodielectric multilayers that sidesteps the time constraints involved with layer-by-layer deposition. In addition, the use of single bilayers inherently improves the uniformity between the individual layers of the rolled stack. Optical-spectroscopy measurements confirm our predictions of stopbands and Bragg resonances and a transfer matrix model of the optical field distribution clearly explains their origin. The high sensitivity of these resonances works to our advantage as any deviations in layer thickness can be easily identified. Although in this particular example our multilayer was Bragg arranged, alternative dimensions are easily used. In particular, the thickness of the polymer layer can be reduced further, although from a fabrication point of view this decrease in film thickness introduces a new complication, in that the film becomes significantly more difficult to manipulate. This can be overcome by increasing the molecular weight of the PS: the polymer chains become more entangled and the strength of the film is improved. This also opens the possibility for further configurations such as concertinas. It would be desirable to bring the polymer-layer thickness down to the same order of magnitude as the metal layer, in order to develop an anisotropic permittivity within the medium, leading to potential sub-wavelength imaging properties. Our cylindrical geometry also offers the potential to extend such an image into the far-field. Light from an object or pattern lying along the central axis of the roll is magnified as it passes through the structure with the evanescent components supported, and once the image has been enlarged above the diffraction limit, it can then be resolved by a conventional microscope in the far-field.[18] Alternatively, our films could be rolled around a hollow capillary tube allowing the real-time imaging of a flow of nanoparticles or colloids. While the radius of curvature of our roll structures is in the millimeter scale here, this is not a fundamental constraint, and we are working towards micrometer-diameter rolls. At these diameters, mechanically controlled roll-up is not possible, and a self- or directed-assembly approach must be employed. Previous work has reported strain-induced roll-up of semiconductor-stacked systems,[19–22] where the lattice mismatch between layers induced roll-up. A similar self-assembly mechanism is possible in metallodielectric systems by swelling the polymer layer,[23] either by temperature expansion or by laser crosslinking of the polymer chains. Fine control over the degree of swelling influences the radius of the rolls, and hence the number of layers in the final structure. This induced-roll-up technique removes the need for a central rod and also improves the scalability of this process. Hence, mass-scalable fabrication (together with lateral structure) is achievable.

Experimental

Surface-Roughness Measurements: The surface roughness of both the PS and the Au layers were measured using a Dimension Atomic Force Microscope, which scanned across a 10 μm × 10 μm area.

Spectroscopy Measurements: The sample was characterized optically using a modified Olympus microscope with a confocally arranged collection of fibers sending light to an Ocean Optics spectrometer.

Acknowledgements

This work was supported by EPSRC grant EP/C511786/1 and Kodak. This article is part of a Special Issue celebrating the 800th Anniversary of Cambridge.

Received: February 10, 2009
Revised: May 20, 2009
Published online: July 20, 2009

[1] J. B. Pendry, *Phys. Rev. Lett.* **2000**, *85*, 3996.
[2] J. B. Pendry, S. A. Ramakrishna, *Phys. B* **2003**, *338*, 329.
[3] C. Montcalm, P. A. Kearney, J. M. Slaughter, B. T. Sullivan, M. Chaker, H. Pépin, C. M. Falco, *J. Opt. A* **1996**, *35*, 5134.
[4] N. Fang, H. Lee, C. Sun, X. Zhang, *Science* **2005**, *308*, 534.
[5] O. Schumacher, S. Mendach, H. Welsch, A. Schramm, C. Heyn, W. Hansen, *Appl. Phys. Lett.* **2005**, *86*, 143109.
[6] C. Deneke, W. Sigle, U. Eigenthaler, P. A. van Aken, G. Schutz, O. G. Schmidt, *Appl. Phys. Lett.* **2007**, *90*, 263107.
[7] M. J. Bloemer, M. Scalora, *Appl. Phys. Lett.* **1998**, *72*, 1676.
[8] M. J. Bloemer, G. D'Aguanno, N. Mattiucci, M. Scalora, N. Akozbek, *Appl. Phys. Lett.* **2007**, *90*, 174113.
[9] M. Scalora, G. D'Aguanno, N. Mattiucci, M. J. Bloemer, D. de Ceglia, M. Centini, A. Mandatori, C. Sibilia, N. Akozbek, M. G. Cappeddu, *Opt. Express* **2007**, *15*, 508.
[10] N. N. Lepeshkin, A. Schweinsberg, G. Piredda, R. S. Bennink, R. W. Boyd, *Phys. Rev. Lett.* **2004**, *93*, 123902.
[11] B. Wood, J. B. Pendry, D. P. Tsai, *Phys. Rev. B* **2006**, *74*, 115116.
[12] D. Melville, R. Blaikie, *Opt. Express* **2005**, *13*, 2127.
[13] I. I. Smolyaninov, *J. Opt. A* **2005**, *7*, 165.
[14] I. I. Smolyaninov, Y. J. Hung, C. C. Davis, *Science* **2007**, *315*, 1699.
[15] V. G. Veselago, *Sov. Phys. Usp* **1968**, *10*, 509.
[16] A. A. Zharov, I. V. Shadrivov, Y. S. Kivshar, *Phys. Rev. Lett.* **2003**, *91*, 37401.
[17] A. K. Popov, V. M. Shalaev, *Appl. Phys. B: Lasers Opt.* **2006**, *84*, 131.
[18] Z. Liu, H. Lee, Y. Xiong, C. Sun, X. Zhang, *Science* **2007**, *315*, 1686.
[19] V. Y. Prinz, V. A. Seleznev, A. K. Gutakovsky, A. V. Chehovskiy, V. V. Preobrazhenskii, M. A. Putyato, T. A. Gavrilova, *Phys. E* **2000**, *6*, 828.
[20] V. Y. Prinz, *Microelectron. Eng.* **2003**, *69*, 466.
[21] V. Y. Prinz, *J. Surf. Invest.* **2008**, *2*, 12.
[22] O. G. Schmidt, K. Eberl, *Nature* **2001**, *410*, 168.
[23] V. Luchnikov, O. Sydorenko, M. Stamm, *Adv. Mater.* **2005**, *17*, 1177.